On the existence, formation and stabilization of Lyne vortices in helically coiled reactors at moderate Reynolds numbers

Conrad Müller[1*], Péter Kováts[1], Katharina Zähringer[1]

1: Laboratory of Fluid Dynamics and Technical Flows, Otto-von-Guericke-Universität Magdeburg. Universitätsplatz 2, D-39106 Magdeburg, Germany.Tel.: +49 391 - 67 58654, Fax: +49 391 - 67 52840

* Correspondent author: conrad.mueller@ovgu.de

Keywords: helically coiled reactors, Dean vortices, Lyne instability, two-phase flow, LIF, PIV

ABSTRACT

The occurrence of Dean and Lyne vortices in curved and coiled tubes is widely known. This paper is on the tracks of vortex structures in more resent helically coiled reactors, namely the Coiled-Flow-Reverser (CFR) and the Coiled-Flow-Inverter (CFI). Time-resolved laser induced fluorescence (LIF) and time-resolved particle image velocimetry (TR-PIV) are used to characterize the existence of Lyne vortices in a range of Reynolds numbers from 500 to 2400 for single phase liquid-liquid mixing flows. In this study parameters like the Reynolds number, the inlet angle and the geometry of the helically coiled reactor are varied and their influence on the vortex occurrence and the mixing coefficient is shown. The results are then compared to two-phase flow structures in helical pipes from Müller et al. (2021), in which secondary and tertiary vortices inside the liquid plugs exist as well. Two transition points for the formation of Lyne vortices in the CFI could be characterised. While Lyne instabilities occur in straight horizontal helix geometries at Reynolds numbers above 1000, in the CFI the first Lyne vortices formed at a Reynolds number of 560. From a Reynolds number of 1600 onwards, these begin to break off, whereby the Lyne vortices continue to occur continuously but no longer steadily. Pseudo-3D reconstructions of the flow in the CF and the CFI are used to show the flow behaviour and the occurrence of Lyne instabilities for different conditions.

1. Introduction

Curved and coiled pipes are frequently used in both laboratory and industrial applications, because complex secondary flow structures can be achieved with low energy costs. These secondary flow structures affect strongly radial mixing and enhance mass transfer as well as heat transfer compared to those of a straight pipe (Kováts et al. 2018, Vashisth et al. 2008). These curvature-induced flows have been studied in the early 20th century by Eustice (Eustice 1911) and many other researchers. The most comprehensive studies have been carried out by Dean (Dean 1927, Dean 1928). He concluded, that the flow in curved pipes is influenced by the centrifugal force, which results in secondary flow structures and in the cross-sectional plane of the pipe two counter rotating vortices, currently known as Dean vortices, appear. These flow structures were further investigated in pulsatile flows by Lyne (Lyne 1971). He has found, that at high Womersley numbers, which is the ratio of transient inertial force and viscous force, an additional pair of vortices coexists with the Dean vortices near to the outer (concave) wall of the curved section. These are the so-called Lyne vortices. The existence of the Lyne instability with four vortices was validated numerically by Dennis and Michael (Dennis and Michael 1982) for steady laminar flows in curved pipes. They have found, that above a critical Dean number (De > 956) a four vortex pattern appears in the calculation results. However, this pattern is unstable against disturbances and ends up in the two-vortex Dean pattern (Yanase et al. 1989). These complex secondary flow pattern later received more attention in medical flow applications e.g. (Pedley 2003, Guha and Pradhan 2017). In the context of two-phase flows, the flow structure in curved and helical pipes is seldomly analysed. Numerically they have been investigated in (Falconi et al. 2016, Krieger et al. 2020, Mansour et al. 2020). Experiments by micro-PIV in planar horizontal curved pipes have been performed by (Zaloha et al. 2012). These showed vortical structures close to the bubbles and triangular vortex structures inside the plug. Recently the authors of this study published a paper concerning mixing behaviour of two-phase flows in helical pipes, that also included the study of the corresponding flow structures (Müller et al. 2021). Some of those results will be used here for comparison with the single phase flow structures.

In the present study the appearance, frequency and stability of the above mentioned Lyne vortices were investigated with laser induced fluorescence (LIF) and particle image velocimetry (PIV) through liquid/liquid and liquid/liquid/gas experiments. These were carried out in different three-turn helical coil geometries at different Dean numbers (Fig. 1), which are all smaller than the critical value found by Dennis and Michael (1982).

CF (standard helix)	CFR (Coiled Flow Reverser)	CFI (Coiled Flow Inverter)
3-coil configuration		

Fig. 1: Geometries of the helix configurations used in the study for single phase measurements.

2. Experimental setup and image postprocessing

A detailed experimental description of the set-ups used in this study can be found in (Kováts et al. 2020) and for the two-phase flows in (Müller et al. 2021). The three-turn helically coiled reactors were made of fluorinated ethylene propylene (FEP) tubes. For the single phase measurements, the tubes with an inner pipe diameter of d = 10 mm and a wall thickness of s = 1 mm were coiled around a polyvinyl chloride (PVC) core pipe with an outer diameter of D = 118 mm and a pitch of b = 16 mm, to obtain the different aspects of each reactor, respectively the 90° bending for the CFI (Fig. 1). The reversion of the CFR was introduced after the 1st and 2nd full turn, as well as for the inversions for the CFI. With laser induced fluorescence (LIF) Reynolds numbers from 600 to 1200 have been examined, while in the case of Particle Image Velocimetry (PIV) measurements have been performed in the range of Reynolds numbers from 500 to 2400, corresponding to Dean numbers for LIF measurements of 175 to 349 and for PIV measurements of 146 to 699.

For two-phase flows, a smaller, only simple coiled horizontal helix reactor (CF) was used with an inner diameter of d_i = 4 mm, a coil pitch of p = 6 mm and a coil diameter of D = 42 mm. This geometry has been chosen due to experimental constraints for the realization of the gas-liquid flow. Total Reynolds numbers from $300 < Re_{total} < 1088$ have been examined in this case, corresponding to Dean numbers between 96 and 340.

a) b)

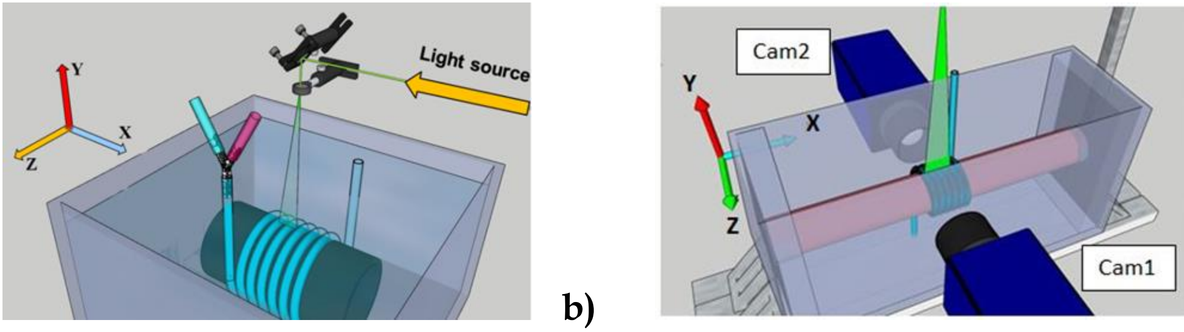

Fig. 2: Experimental set-ups for the single-phase case (a) and two-phase case (b).

In all cases, the reactors were placed into an acrylic box (Fig. 2) filled with 5.25 m% glycerol-water solution, whose refractive index was adjusted to the FEP tube material, to reduce the light refraction on the curved surfaces of the helices. The same solution was used as working liquid for the PIV measurements, whereas for LIF, no adjustment of the refractive index of the working fluid could be realized, due to chemical incompatibilities. The flow is driven by gravity from two 150 l tanks, each situated about 3 m above the reactors and regulated by needle valves. For LIF, one of the tanks was filled with de-ionized water, whereas in the other tank de-ionized water was marked by the fluorescent tracer resorufin. Both fluids were used in the same quantity. For PIV, the liquid of one tank is guided through the same tubing system as for LIF, in order to keep the same pressure losses.

As light source a pulsed Nd:YAG laser with 532 nm was applied for the single-phase LIF measurements and the light sheet crosses the tubes on top of the reactors (Fig. 2). Perpendicular to the illuminated cross sections, a scientific CMOS camera (Imager sCMOS, 2560x2160 pixels) with a 100 mm Tokina macro lens was mounted. The excitation light was filtered with a 555 nm high pass filter and only the fluorescence intensity of resorufin was acquired. With this setup, 500 images with 15 Hz recording rate have been recorded for each inlet condition.

For PIV measurements in the single phase flow, rhodamin B doped tracer particles with a mean diameter of 20 µm were excited with a high-speed Nd:YLF laser at 527 nm. 1000 images have been recorded with an Imager Pro HS 4M high-speed camera (2016x2016 pixels). On the camera a 100 mm Tokina macro lens with a 537 nm long pass filter was mounted. Since these recordings were time-resolved, the recording rate and therefore the time delay between the images was set according to the flow rate.

In the case of the two-phase flow, the fluorescence of resorufin (for mixing) and rhodamin B particles (for PIV) were excited by the same high-speed laser at 527 nm. The fluorescence intensities were also detected with two Imager Pro HS 4M high speed cameras, each using an AF Micro Nikkor 60 mm lens with a 537 nm long pass filter. The image capturing and processing approach allowed in this case the reconstruction of pseudo-3D mixing and flow fields. The corresponding procedures, which are not the scope of this paper, are described in detail in (Müller et al. 2021).

For the determination of the effect of the Lyne vortices on the mixing quality, mixing coefficients are calculated according to Eq. (1):

$$M_c = 1 - \frac{\sum_f |c - \bar{c}_{inlet}| A_f}{|\bar{c}_{inlet}| \sum_f A_f} \tag{1}$$

with $$\bar{c}_{inlet} = \frac{1}{A} \int c_{inlet}\, dA$$

where c is the local concentration of the tracer, $\bar{c}$ the average concentration over the cross-sectional area A under inlet conditions (representing the expected value for perfect mixing), and A_f is the area of a grid unit. The mixing coefficient has a range from 0 to 1, where 0 shows the case of no mixing and 1 refers to perfect mixing. The concentrations are directly proportional to the fluorescence intensity of resorufin for the concentration used here (Kováts et al. 2018). Thus a normalization with the maximum value at maximum concentration and a background subtraction are sufficient for postprocessing. The mixing coefficient can then be calculated with the above mentioned equation (Eq. 1).

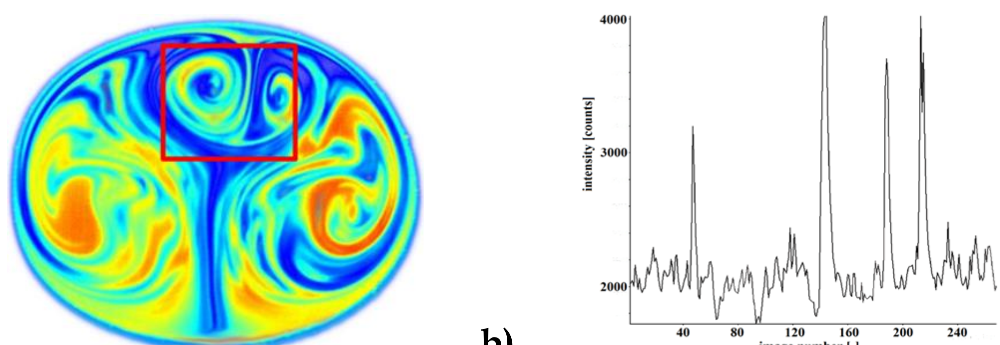

a) b)

Fig. 3: Investigation window for the vortex recognition (a) and average intensity change in that window over an exemplary image set of 250 images (b). Four vortices are recognized and counted in this example.

During image processing, the illuminated cross-sections were masked out from the fluorescence images and vortex recognition could be realized automatically. To this end, an investigation window was selected in the cross sectional image close to the outer (here upper) wall of the helix (Fig. 3, a), where the Lyne vortex pair appears (red rectangle in Fig. 3). The presence of a vortex pair causes an intensity peak in the image and allowed for the counting of the generated vortices in the recorded image series (Fig. 3, b). In the following, the intensity images are represented with a colour scale ranging from deep blue for pure water, over light green (ideal mixing, Mc = 1), to red for the initial resorufin concentration (1 mg/l).

In all time-resolved PIV measurements (single and two phase flow), a geometric mask, in the form of the tube walls, was used to remove disturbances outside the measuring area, as, for example, reflections on the tube walls. The vector calculation was then done with a multi-pass cross-correlation with decreasing interrogation area size, starting from 64×64 pixels with 50% overlap for the first 2 passes and reduced to 32×32 pixels with 50% overlap for the next 4 passes. Vector post-processing includes a median filter and an iterative replacement of excluded vectors. These were interpolated from their neighbours, and an optimal smoothing was applied. In the case of single phase flow, a mean flow field was calculated from 1000 instantaneous flow fields (Fig. 4).

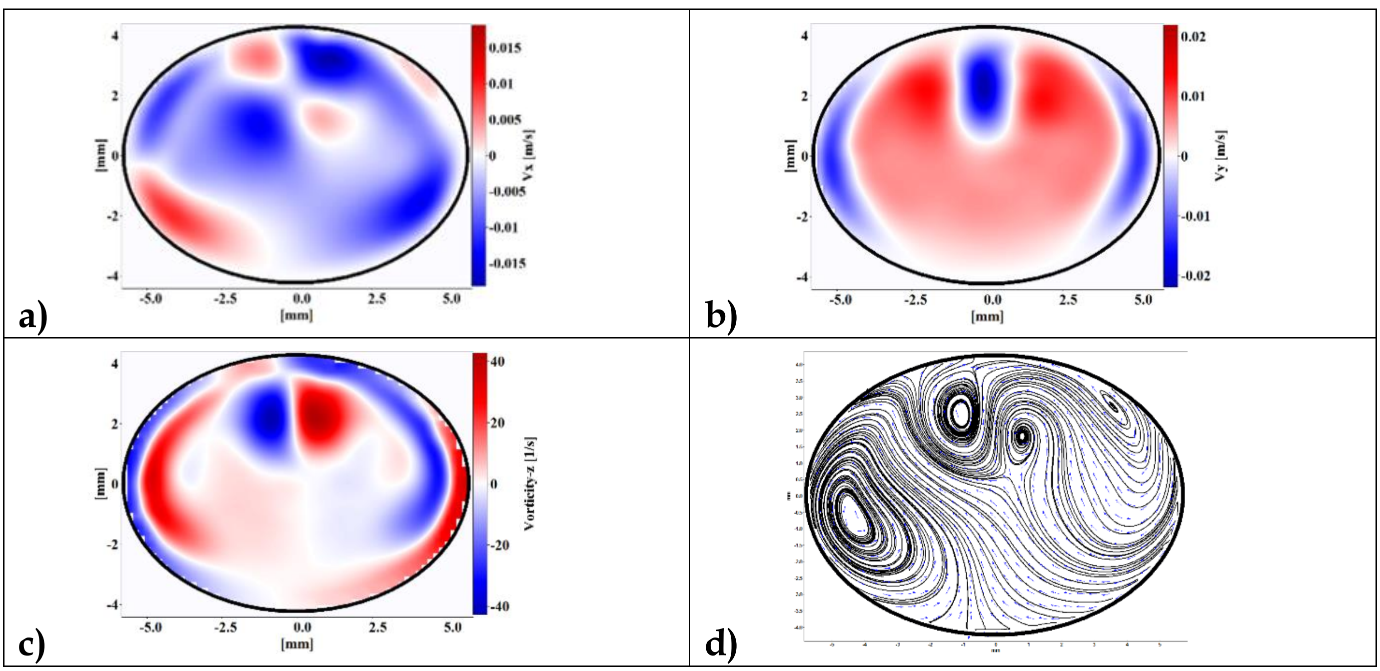

Fig. 4: Exemplary mean flow fields from the single phase PIV measurements at Re = 750 showing the horizontal velocity component (a), the vertical velocity component (b), the vorticity in z-direction (c) and the stream lines in the second turn of the CFI.

3. Results and Discussion

The following section will discuss the occurrence of secondary vortex structures in helically coiled reactors and their influence on the mixing coefficient, calculated with Eq. (1), from time resolved LIF measurements in the range of Re = 600…1200. Furthermore, the transition from Dean vortices to Lyne vortices is investigated by PIV measurements in the range of Re = 500…2400. Single phase liquid-liquid mixing is then compared to two-phase cases from Müller et al. (2021).

3.1 Occurrence of Lyne Vortices

As described in section 2 and Fig. 3 the occurrence of secondary vortex structures is mapped in the following images for different Reynolds numbers and geometries (CF, CFR and CFI) on top of the first and the second coil of the helical reactors, so 270° and 630° after the inlet respectively. The influence of the inlet angles vertical to the flow direction were also investigated. Therefore, the inlet angles were set to a = -4.5°, 0°, 4.5 and β°= -5°, 0°, 5. However, it turned out that inlet angles in the investigated range of angles, close to a straight inlet configuration, have no mandatory influence on the flow inside the helix. Only very rarely the inlet angles can provoke different vortex structure outcomes at constant Reynolds number, which is shown later. So, it became clear that the creation of secondary vortex structures in all geometries is mainly dependent on the Reynolds number with differences between the three geometries.

The vortex structures found in the helix reactors can be split into 4 cases as shown in Fig. 5, which are: steady Dean vortices (a), additional unsteady Lyne vortices, appearing only occasionally (b), additional steady Lyne vortices (c) and more turbulent vortex structures (d).

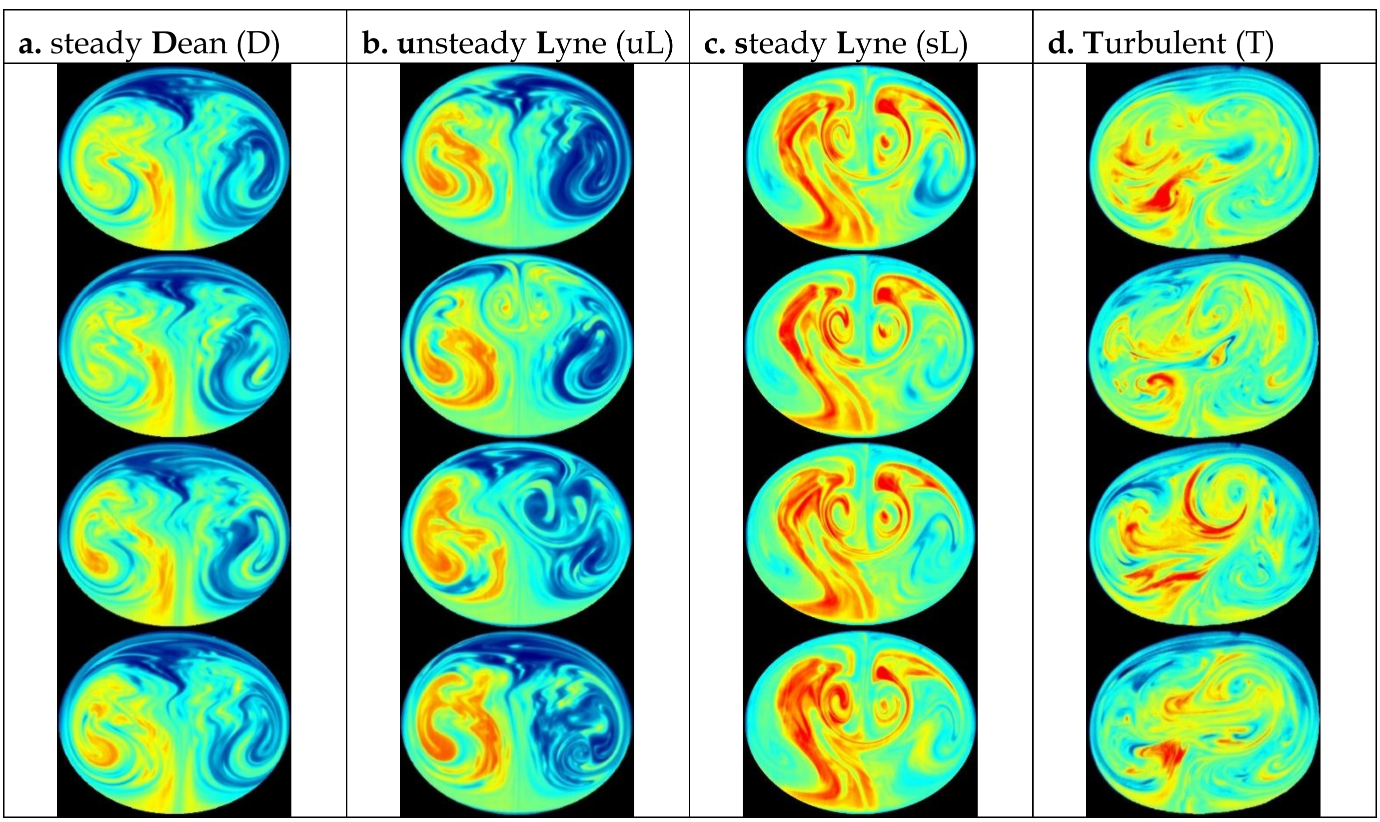

Fig. 5: Examples of possible flow cases for Re = 1000 in the helical reactors. From left to right: steady Dean vortices (D), unsteady Lyne vortices (uL), steady Lyne vortices (sL), turbulent vortex structures (T).

In the following Table 1, the existence of Lyne vortices is mapped in function of the geometry and the Reynolds number. Therefore, the occurrence of the 4 cases of possible vortical flows (Fig. 5) are listed for different Reynolds numbers. In the first coil of all geometries unsteady Lyne vortices appear only at Reynolds numbers higher than Re = 1000. The CFR creates more turbulent vortex structures already at *Re* = 800 after the first turn where the flow gets reversed by 180°. In the second coil of the CFI, where the flow gets inversed by 90°, the geometry seems to have a stabilizing effect on the Lyne vortex structures even at lower Reynolds numbers, creating steady Lyne vortices being recognizable in all images, as shown exemplary in Fig. 5 c.

Table 1: Occurrence of Lyne vortices in helical reactors in function of the Reynolds number (for abbreviations see text and Fig. 5

Re	CF		CFR		CFI	
	Coil 1	Coil 2	Coil 1	Coil 2	Coil 1	Coil 2
600	D	D	D	D	D	sL
800	D	D	D	T	uL (sL)	sL
1000	uL	uL	D (uL)	T	uL	sL
1200	uL	uL	uL	T	uL	sL

3.2 Mixing Coefficient

Compared to the Dean vortices, the Lyne vortices add some additional structure to the flow field. Their influence on mixing in the cross-section of the first coil of the helix reactors is shown in Fig. 6 - Fig. 8 for constant Reynolds numbers and different inlet angles. Marked in red are the time steps in which Lyne vortices are visible. In the first coil of all geometries (CF, CFR and CFI) mainly unsteady Lyne vortices were found. Changes of the inlet angle lead to cases without Lyne vortices in the CFR at 0° (Fig. 7 b) and CFI at 4.5° (Fig. 8 c) and to almost continuous but still unstable Lyne vortices in the CFI, which can only be seen in the images where after a Lyne vortex collapses a new one appears immediately after (Fig. 8 a and b). Cases with Lyne vortices have a higher fluctuation in the mixing coefficient, but the average mixing coefficient over the whole measurement cycle stays the same.

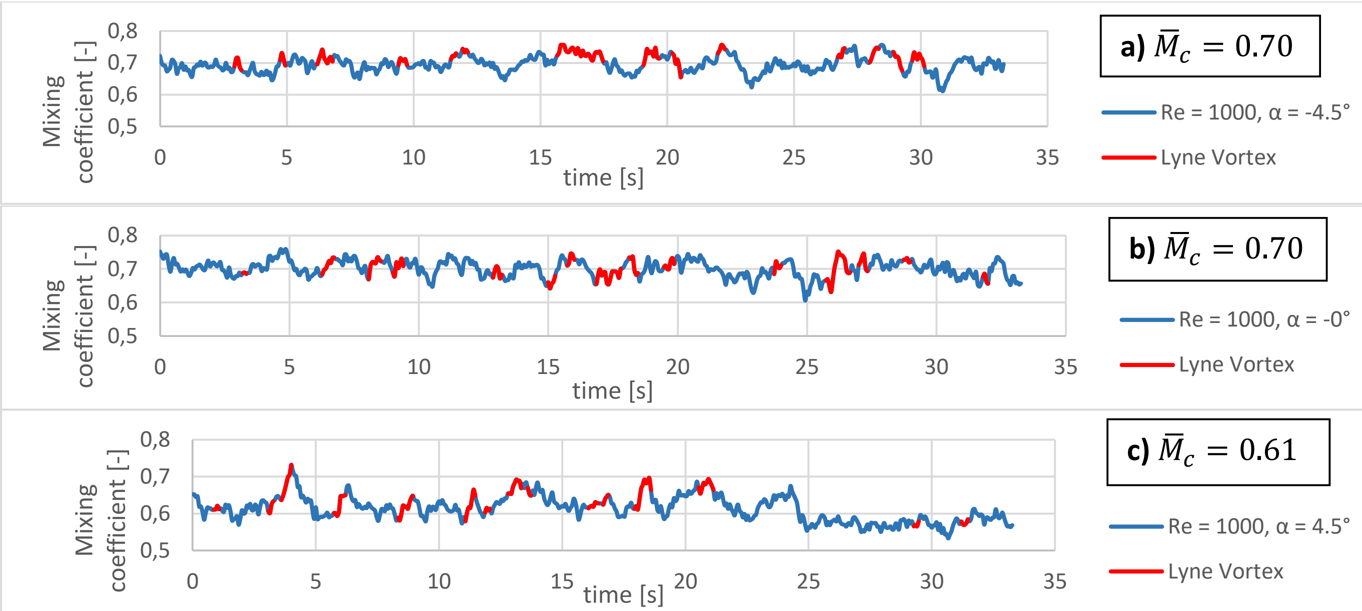

Fig. 6: Exemplary temporal mixing coefficient in the first coil of the CF of single phase LIF measurements at *Re* = 1000 for different inlet angles *α*. The occurrence of Lyne vortices is marked in red.

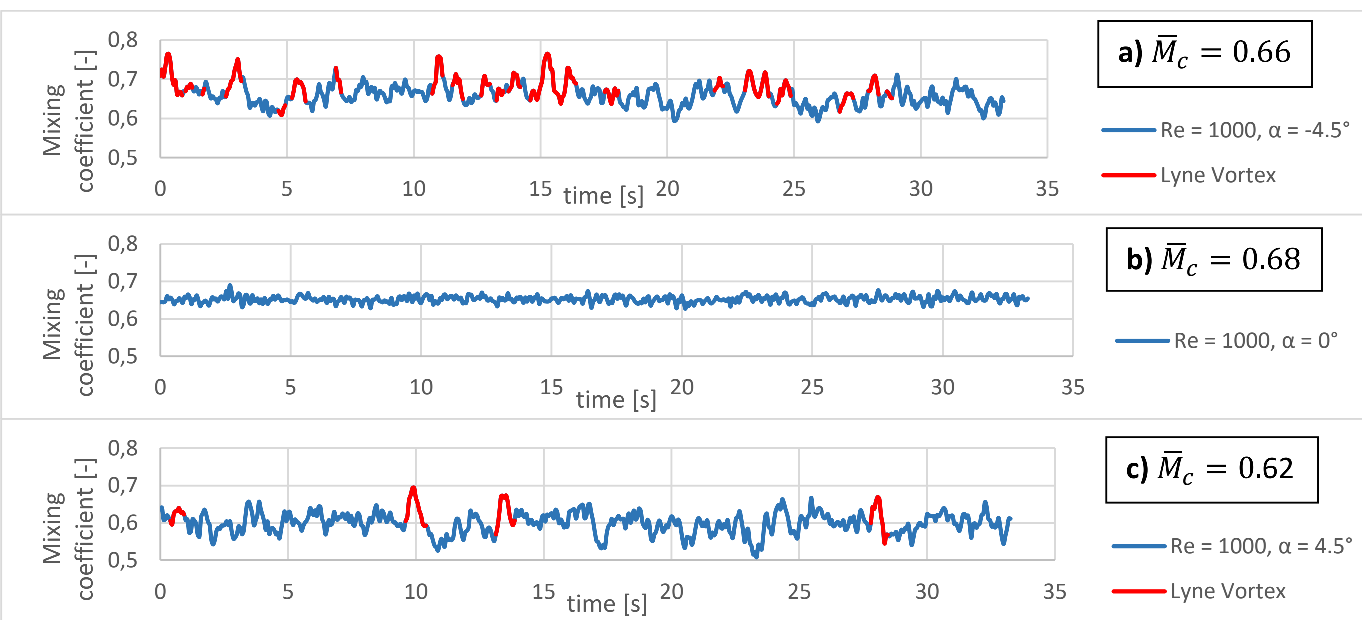

Fig. 7: Exemplary temporal mixing coefficient in the first coil of the CFR of single phase LIF measurements at *Re* = 1000 for different inlet angles *α*. The occurrence of Lyne vortices is marked in red.

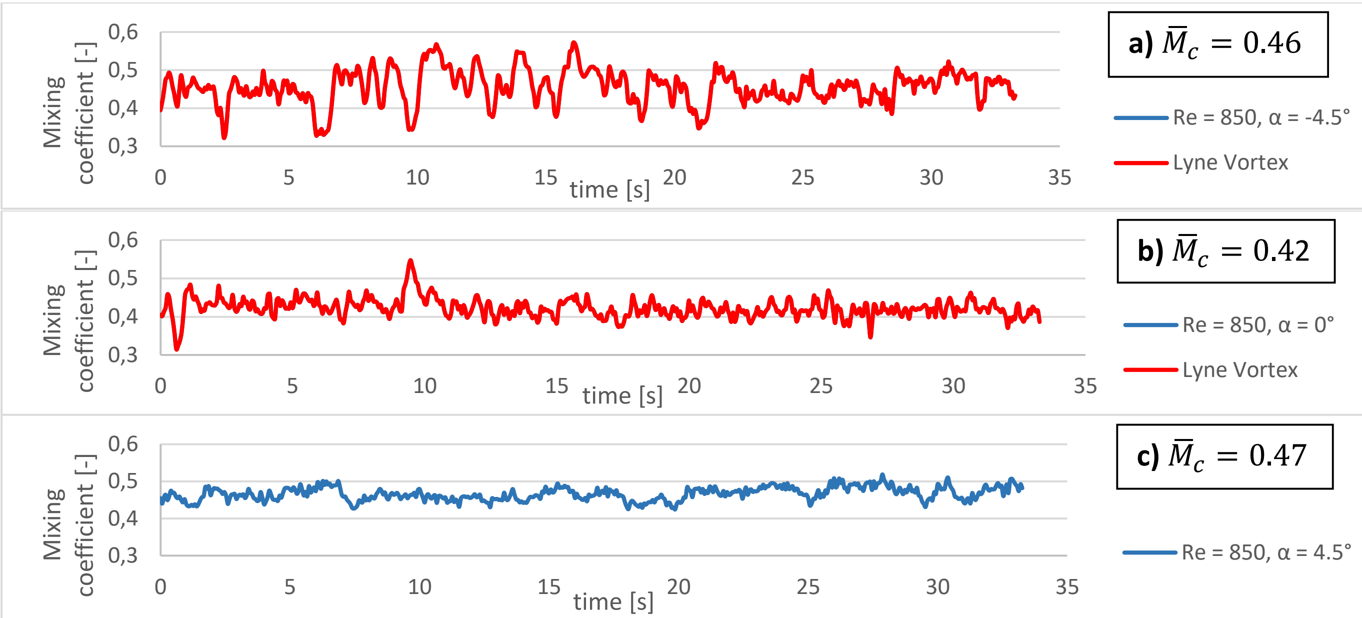

Fig. 8: Exemplary temporal mixing coefficient in the first coil of the CFI of single phase LIF measurements at *Re* = 850 for different inlet angles *α*. The occurrence of Lyne vortices is marked in red.

In the following Fig. 9 the time-resolved mixing coefficient in the second coil of the different geometries is shown. Here, the geometrical redirections of the flow are situated upstream of the measuring cross-section and the differences between the geometries become more important. The CF shows mainly unsteady Lyne vortices, the CFR more turbulent vortex structures and the CFI steady Lyne vortices (see Table 1). The inlet angle has no effect on the flow anymore and therefore only the straight inlet configuration (0°) is shown.

The turbulent vortex structures seen in the CFR (red lines) lead always to the best mixing conditions at each Reynolds number. On the other hand, the steady Lyne vortices in the CFI (black lines), trap the liquid, which leads to a poor mixing quality. At high Reynolds numbers (full lines) the differences in mixing of the CF, CFR and CFI become negligible.

Fig. 9: Exemplary temporal mixing coefficient in the second coil of the CF, CFR and CFI for single phase LIF measurements at different Reynolds numbers with a straight inlet.

3.3 Flow Field (PIV)

The PIV measurements were carried out for Reynolds numbers between 500 and 2400 in order to determine the transition point at which Lyne vortices first stabilize in the helically coiled reactors. The PIV results in single phase flow showed also, that the additional vortex pair in the CF reactor exists but is not stable even when going to Reynolds numbers up to 2400. Fig. 10 shows an example flow field at Re = 2000. The additional vortex pair can be found on some instantaneous vorticity fields, like Fig. 10 a, but on the mean vorticity field it nearly disappears and only a very small vortex pair can be recognized near the outer wall (top of the image) (Fig. 10, b).

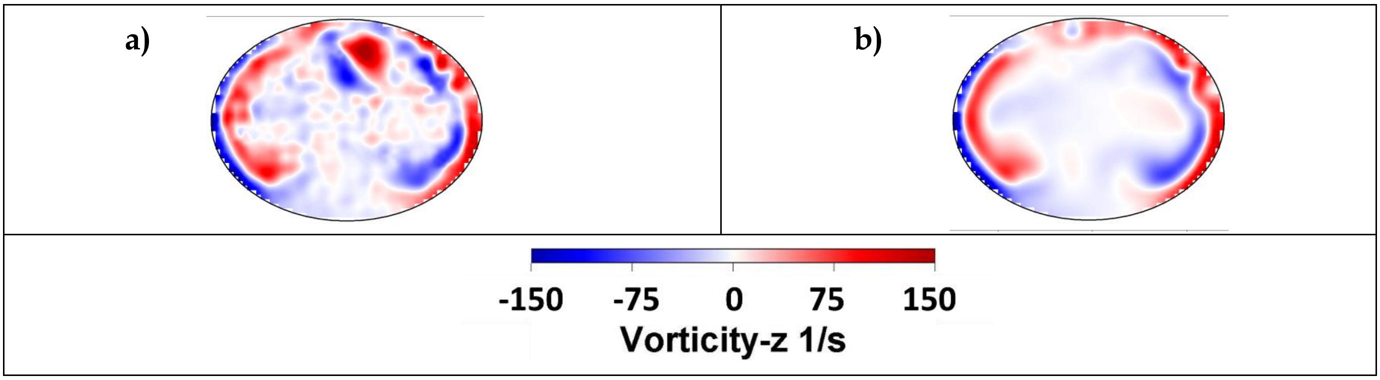

Fig. 10: Exemplary instantaneous (a) and mean (b) vorticity fields in the 1st cross-section for single phase flow in the CF reactor at *Re* = 2000.

Contrarily, the CFI geometry stabilizes this additional vortex pair in the second coil. From around Re = 560 a weak vortex pair appears near the outer wall (centre top of Fig. 11, b, inside the black rectangle) and with increasing Reynolds number, this vortex pair becomes stronger and bigger and with this, the cores of the vortices move to the centre of the tube (Fig. 11 c and d). At higher Reynolds numbers above *Re* = 1700 the Lyne vortex pair becomes deformed and smeared (Fig. 11 e) indicating unsteady behaviour.

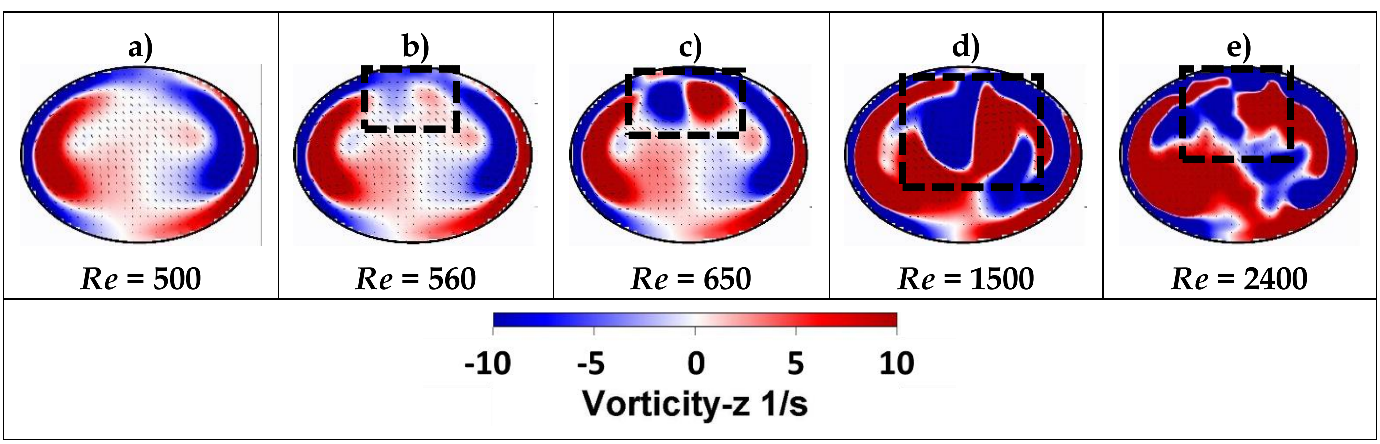

Fig. 11: Exemplary mean vorticity fields in the second turn of the CFI reactor at different Reynolds numbers.

In the following Fig. 12, unrolled pseudo-3D reconstructions of the flow field (see Müller et al., 2021 for the post-processing to obtain these) of the CF and the CFI are shown in a top view projection for selected Reynolds numbers, to exemplify the time resolved behaviour of the flow. The CF shows mostly steady Dean vortices. At Reynolds numbers of *Re* = 1700 and *Re* = 2000 some unsteady Lyne vortices are visible, increasing in appearance frequency with increasing Reynolds number, but also becoming more turbulent. In the CFI, at a Reynolds number of 500 only steady Dean vortices are visible, but already at *Re* = 560 up to *Re* = 1500 steady Lyne vortices are developing in between. At *Re* = 1600 the Lyne vortices start wiggling, creating a wavy structure, which are later breaking apart at *Re* = 1700 showing unsteady behaviour from this point on. The overall vortex occurrence in the CFI is higher compared to the CF and even at the highest measured Reynolds numbers clear structures can be detected.

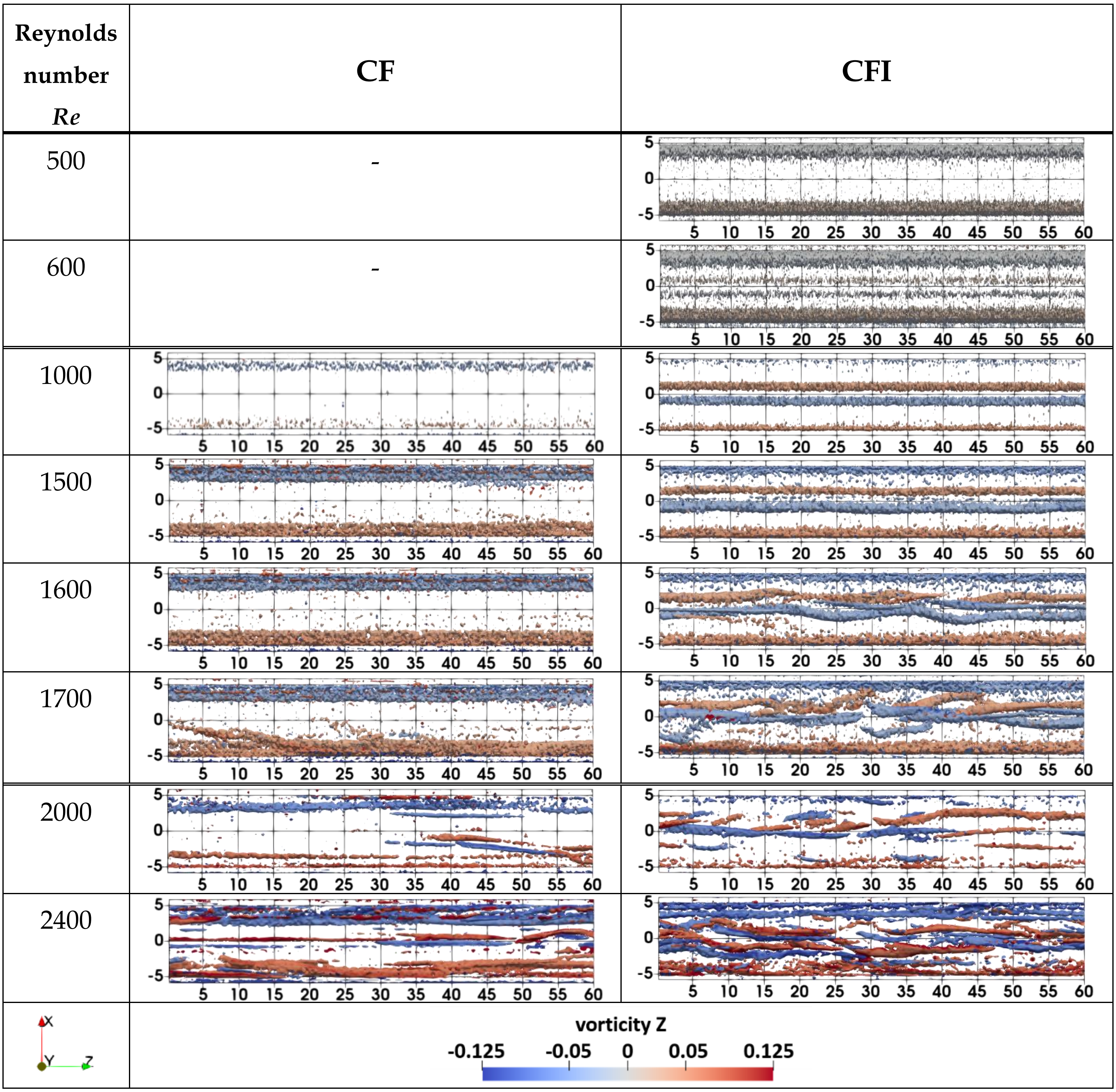

Fig. 12: Unrolled top view of pseudo 3D reconstruction for different Reynolds numbers in the second coil of the CF and CFI. Q-criterion for $Re < 1000$ is $Q = (1.25*10^{-5}\ldots\text{max})$, for $1000 \leqq Re < 2000$ is $Q = (2.5*10^{-4}\ldots\text{max})$ and for $Re \geq 2000$ $Q = (1.0*10^{-3}\ldots\text{max})$, coloured by z-vorticity.

3.4 Comparison to two-phase flow

The PIV results obtained for the two-phase flow showed the establishment of additional vortex pairs, when increasing the Reynolds number (Fig. 13). The Dean vortices always exist as counter-rotating vortices near the tube walls in the liquid plug (here represented in an unrolled manner by an isosurface of the Q-criterion in front of a bubble (grey surface) on top and bottom of the respective images). At lower Reynolds numbers (below *Re* = 500, Fig. 13, a), additional secondary vortices, very near to the bubble (grey surface) and rotating in the same sense as the Dean vortices develop but are shifted to the outside wall of the tube (here towards the reader). At a Reynolds number around *Re* = 650, a third vortex pair forms, counter-rotating compared to the Dean vortices and coexisting to the shifted secondary Dean vortices, clearly visible in Fig. 13 b-d in front of the bubble. With increasing Reynolds number, the counter-rotating vortices, suppress the secondary vortices and coexist with the main Dean vortices (Fig. 13 d). These vortices evoke the Lyne vortices, as seen in the single-phase experiments.

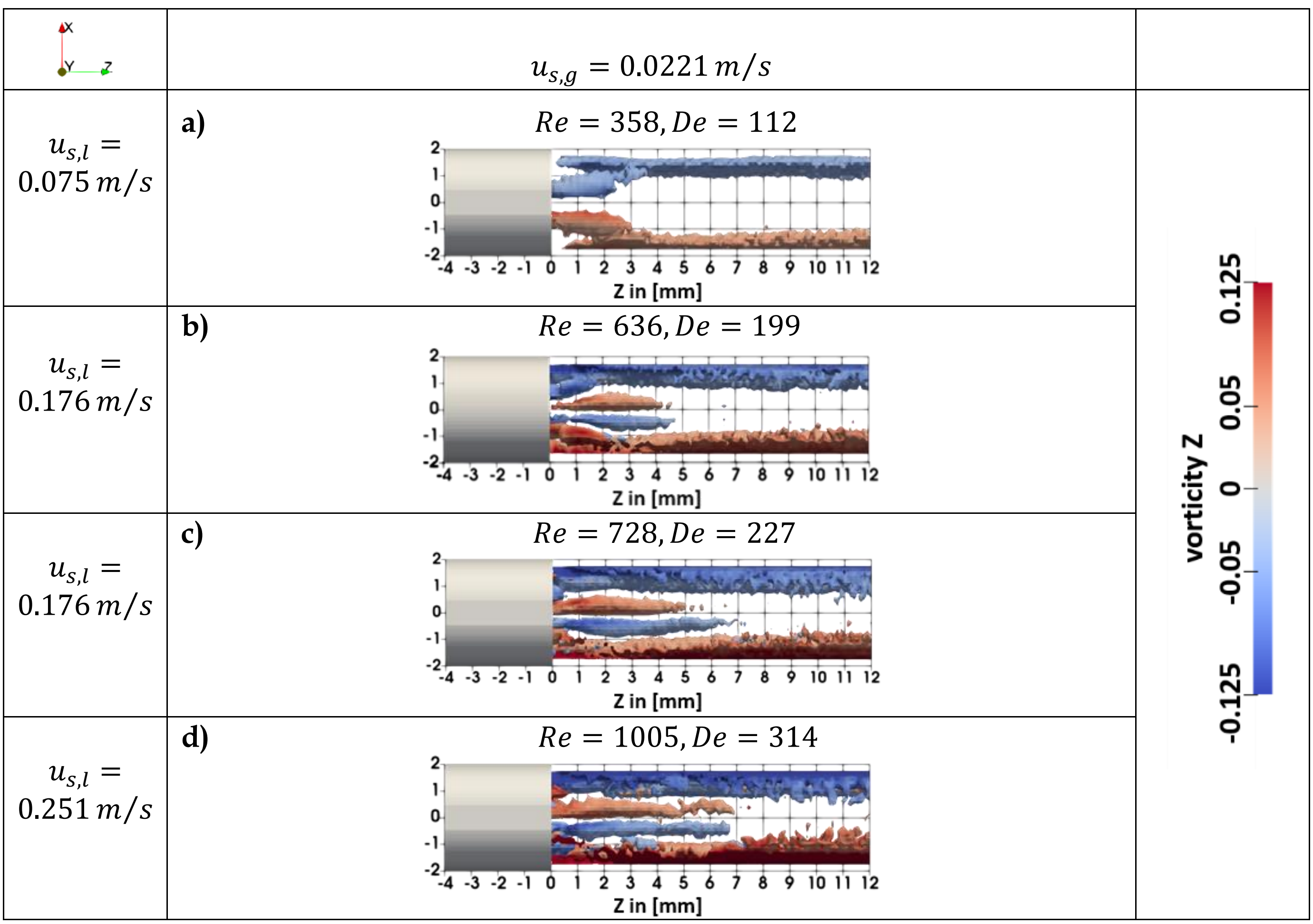

Fig. 13: Mean flow structures 12 mm in front of a bubble (grey) for different liquid velocities, unrolled top view of a part of the liquid plug; isosurface Q-Criterion with $Q = (3.5*10^{-4}\ldots\text{max})$ coloured by z-vorticity.

These vortices are situated in the same position as the Lyne vortices of the single-phase cases, since they are located near the outer wall of the coil, as can be seen on the streamline visualizations in Fig. 14. They appear at about $Re \approx 560$, $De \approx 163$, where in the two-phase case the shifted secondary Dean vortices get suppressed by the Lyne vortices, as in the single-phase flow in the second coil of the CFI geometry. The intermitting bubbly flow seems to induce and stabilize these vortices. However, with increasing Reynolds number the vortices do not tend to move to the centre of the tube, as the Lyne vortices do in the single phase case (Fig. 14). Another difference is, that the additional vortices in front of bubbles increase mixing inside the liquid plug, that has been shown by corresponding LIF measurements (Müller et al. 2021), while the mixing coefficient is unaffected by temporal Lyne vortices in the single-phase case or becomes even worse for steady Lyne vortices. At this point it is important to mention, that the geometrical differences between the single-phase and two-phase cases (see Müller et al. 2021 for details), like the coil diameter and the coil pitch could also influence the observed flow structures.

Single-Phase CFI 2nd loop		 Re = 600	 Re = 800	 Re = 1000
Two-Phase CF 2nd loop	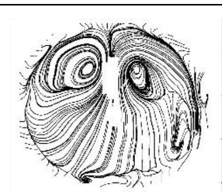 Re = 358	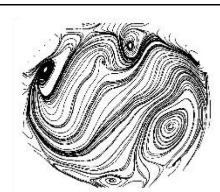 Re = 636	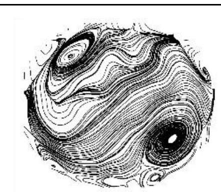 Re = 820	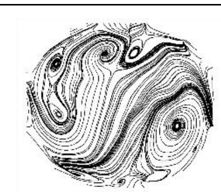 Re = 1005

Fig. 14: Comparison of Lyne vortices for different Reynolds numbers for instantaneous flow fields. Two-Phase case at Re = 358 shows shifted Dean vortices.

4. Conclusions

The present study gives *experimental* evidence on the existence of Lyne vortex pairs in helically coiled reactors also for laminar flow conditions and is able to set transition points for their occurrence. The four-vortex pattern is instable in the straight helical reactor (CF) and becomes more turbulent in the CFR after the flow gets reversed by 180°. However, due to the 90° flow inversion in the CFI reactor, these vortex structures are stabilized in the range of $560 < Re < 1600$, corresponding to Dean numbers between 163 and 466. For higher Reynolds numbers the Lyne vortices are still present, but start to break off and show a very unstable behaviour.

A similar stabilization effect was recognized in gas-liquid flows through a straight helical coil. It was also found that the four-vortex structure has no significant influence on the overall mixing coefficient of liquid-liquid mixing in all investigated reactors, but only increases the fluctuations. Also, temporal Lyne vortices do not cause a temporal maximum of the mixing coefficient. However, Lyne vortices induced by bubbles in the two-phase case increase mixing in the liquid plugs of two-phase flows.

As stated originally by Lyne, the secondary vortices are stabilized through pulsation. In a two-phase flow inside the horizontal helical reactor such pulsation is also created by the bubbles, due to the changes of direction of the buoyancy force. In the single-phase case, this stabilization is only obtained in the CFI geometry, probably due to the recirculation zones, induced after the 90° bends for redirection of the flow.

Acknowledgements

Authors would like to thank the Deutsche Forschungsgemeinschaft (DFG, German Research Foundation) - TRR 63 "Integrated Chemical Processes in Liquid Multiphase Systems" (subproject B1) - 56091768 (Gefördert durch die Deutsche Forschungsgemeinschaft (DFG) - TRR 63 "Integrierte chemische Prozesse in flüssigen Mehrphasensystemen" (Teilprojekt B1) – 56091768).
Our student Daniel Weselmann is acknowledged for his help during the experiments and Yingjie Chang for his help with the processing.

References

Dean WR (1927) XVI.Note on the motion of fluid in a curved pipe. *The London, Edinburgh, and Dublin Philosophical Magazine and Journal of Science* 4:208-223 DOI 10.1080/14786440708564324

Dean WR (1928) LXXII.The stream-line motion of fluid in a curved pipe (Second paper). *The London, Edinburgh, and Dublin Philosophical Magazine and Journal of Science* 5:673-695 DOI 10.1080/14786440408564513

Dennis SCR, Michael NG (1982) Dual Solutions for Steady Laminar Flow through a Curved Tube. *The Quarterly Journal of Mechanics and Applied Mathematics* 35:305-324 DOI 10.1093/qjmam/35.3.305

Eustice J (1911) Experiments on Stream-Line Motion in Curved Pipes. *Proceedings of the Royal Society A: Mathematical, Physical and Engineering Sciences* 85:119-131 DOI 10.1098/rspa.1911.0026

Falconi CJ, Lehrenfeld C, Marschall H, Meyer C, Abiev R, Bothe D, Reusken A, Schlüter M, Wörner M (2016) Numerical and experimental analysis of local flow phenomena in laminar Taylor flow in a square mini-channel. *Physics of Fluids* 28 DOI 10.1063/1.4939498

Guha A, Pradhan K (2017) Secondary motion in three-dimensional branching networks. *Physics of Fluids* 29:063602 DOI 10.1063/1.4984919

Kováts P, Pohl D, Thévenin D, Zähringer K (2018) Optical determination of oxygen mass transfer in a helically-coiled pipe compared to a straight horizontal tube. *Chemical Engineering Science* 190:273-285 DOI https://doi.org/10.1016/j.ces.2018.06.029

Kováts P, Velten C, Mansour M, Thévenin D, Zähringer K (2020) Mixing characterization in different helically coiled configurations by laser-induced fluorescence. *Exp Fluids* 61:203 DOI 10.1007/s00348-020-03035-0

Krieger W, Bayraktar E, Mierka O, Kaiser L, Dinter R, Hennekes J, Turek S, Kockmann N (2020) Arduino-based slider setup for gas–liquid mass transfer investigations: Experiments and CFD simulations. *AIChE Journal* 66 DOI 10.1002/aic.16953

Lyne WH (1971) Unsteady viscous flow in a curved pipe. *Journal of Fluid Mechanics* 45:13-31 DOI 10.1017/s0022112071002970

Mansour M, Landage A, Khot P, Nigam KDP, Janiga G, Thévenin D, Zähringer K (2020) Numerical Study of Gas–Liquid Two-Phase Flow Regimes for Upward Flow in a Helical Pipe. *Industrial & Engineering Chemistry Research* 59:3873-3886 DOI 10.1021/acs.iecr.9b05268

Mansour M, Liu Z, Janiga G, Nigam KDP, Sundmacher K, Thévenin D, Zähringer K (2017) Numerical study of liquid-liquid mixing in helical pipes. *Chemical Engineering Science* 172:250-261 DOI 10.1016/j.ces.2017.06.015

Müller C, Kováts P, Zähringer K (2021) Experimental characterization of mixing and flow field in the liquid plugs of gas–liquid flow in a helically coiled reactor. *Exp Fluids* 62:190 DOI 10.1007/s00348-021-03284-7

Pedley TJ (2003) Arterial and Venous Fluid Dynamics. 1-72 DOI 10.1007/978-3-7091-2542-7_1

Vashisth S, Kumar V, Nigam KDP (2008) A review on the potential applications of curved geometries in process industry. *Industrial & Engineering Chemistry Research* 47:3291-3337 DOI 10.1021/ie701760h

Yanase S, Goto N, Yamamoto K (1989) Dual solutions of the flow through a curved tube. *Fluid Dynamics Research* 5:191-201 DOI 10.1016/0169-5983(89)90021-x

Zaloha P, Kristal J, Jiricny V, Völkel N, Xuereb C, Aubin J (2012) Characteristics of liquid slugs in gas–liquid Taylor flow in microchannels. *Chemical Engineering Science* 68:640-649 DOI https://doi.org/10.1016/j.ces.2011.10.036